SUPPORTING INFORMATION

Affinity Purification and Single-Molecule Analysis of Integral Membrane Proteins from Crude Cell-Membrane Preparations

Anders Lundgren[*,1,2,†,‡], Björn Johansson Fast[1,†], Stephan Block[1,§], Björn Agnarsson[1], Erik Reimhult[2], Anders Gunnarsson[3] and Fredrik Höök[*,1]

[1]Department of Physics, Chalmers University of Technology, 41296 Gothenburg, Sweden

[2]Department of Nanobiotechnology, University of Natural Resources and Life Sciences, 1190 Vienna, Austria

[3]Discovery Sciences, Innovative Medicines and Early Development Biotech Unit, AstraZeneca, 43183 Mölndal, Sweden

[†] These authors contributed equally to this work

[‡] Current address: Department of Chemistry and Molecular biology, University of Gothenburg, 405 30 Gothenburg, Sweden

[§] Current address: Department of Chemistry and Biochemistry, Freie Universität Berlin, 14195 Berlin, Germany

[*] Email: anders.lundgren@gu.se, Tel: +46 (0) 31 786 25 77

[*] Email: fredrik.hook@chalmers.se, Tel: +46 (0) 31 772 61 30

Table of Content

Supporting Figures

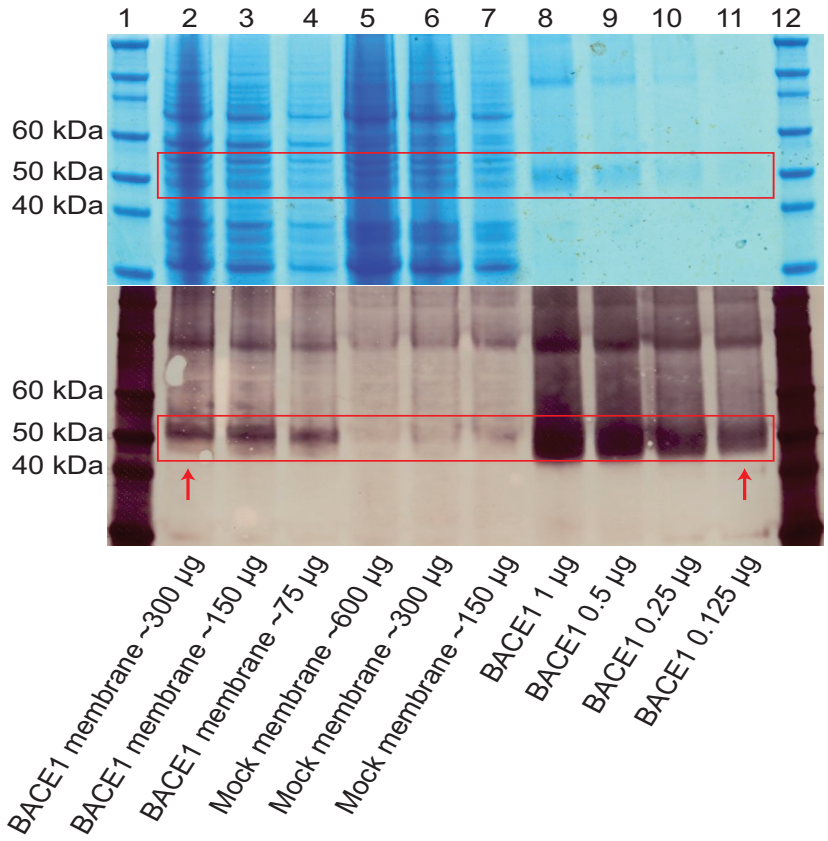

Supporting Figure S1: Estimation of BACE1 content in native membrane vesicles (NMVs). SDS-PAGE (upper) and Western blot (lower) of BACE1 (lane 2-4) and mock (lane 5-7) membrane from cells not expressing BACE1, and dilution series of purified BACE1 (lane 8-11) for calibration. The minor signal from BACE1 in lane 7 is most likely due to spill over from lane 8 during loading of the gels.

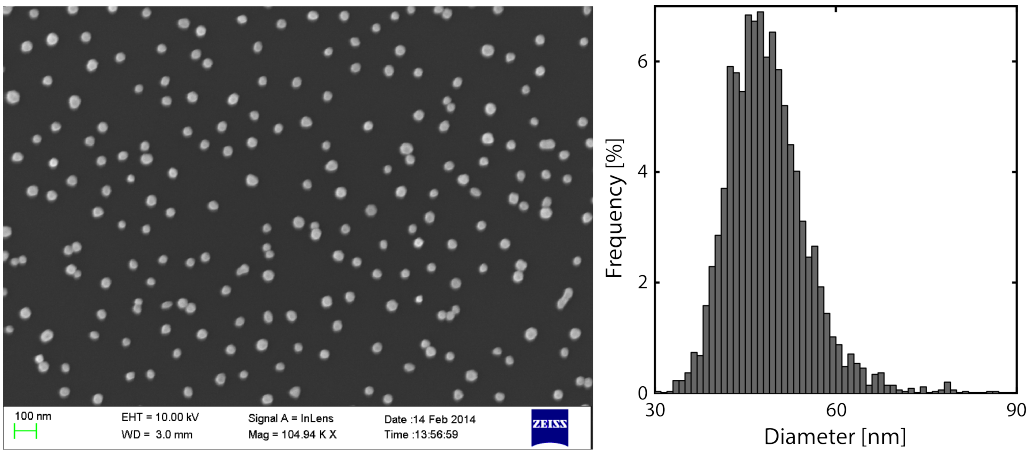

Supporting Figure S2: Electron micrographs of gold NPs obtained by seed-mediated synthesis. Some aggregated NPs can be seen, which appear during sample drying due to capillary forces between closely positioned NPs. The corresponding NP-size distribution is displayed to the right.

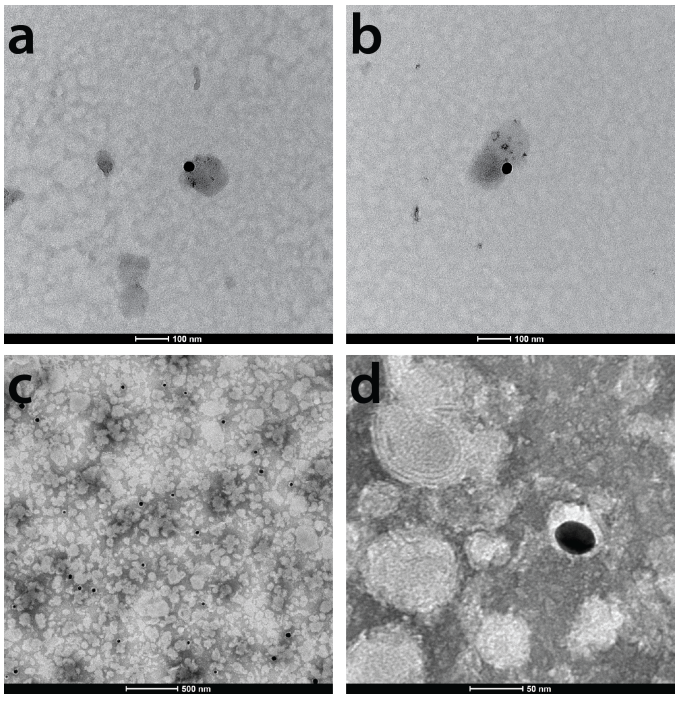

Supporting Figure S3: Transmission electron micrographs of AuNP-NMV constructs. Micrographs obtained from the same sample of NMVs conjugated to antibody-modified AuNPs adsorbed onto grids without (a-b) and with (c-d) PLL pre-treatment and stained with uranylacetate.

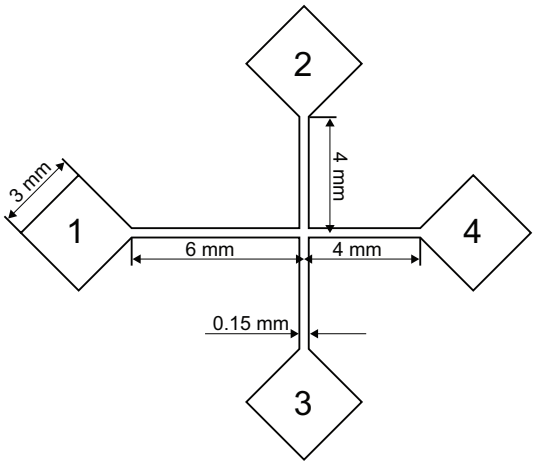

Supporting Figure S4: Schematic illustration of the 4-arm microfluidic device. Numbers indicate the connections. Device height was 110 µm, measured using a profilometer.

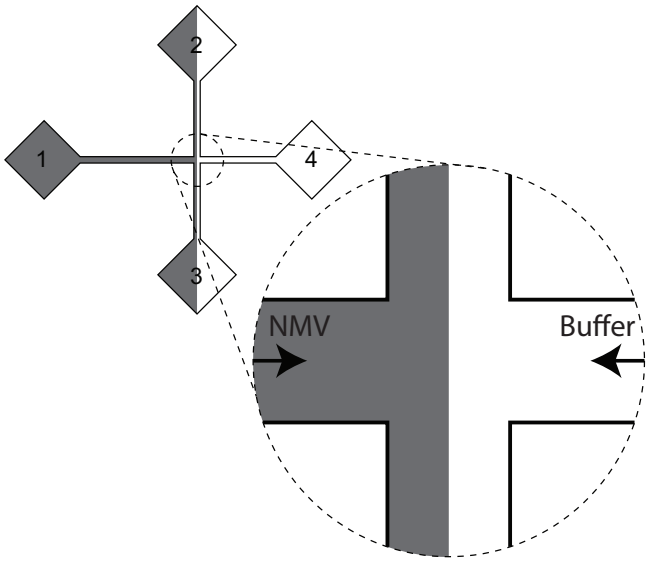

Supporting Figure S5: Schematics illustrating the creation of a membrane edge in the centre of the channel. Membrane material was injected into connection 1, a buffer counter-flow was applied through connection 4, and the outlet connection 2 and 3 were left open. During the accumulation experiments, connections 2 and 3 were closed, while connection 1 was configured as buffer inlet and connection 4 as outlet.

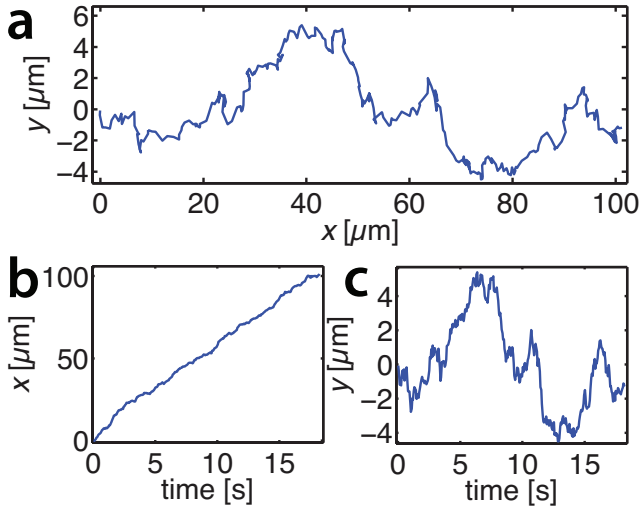

Supporting Figure S6: **Stochastic and deterministic components of NP movement under flow.** Representative trajectory (**a**) of a single NP (hydrodynamic diameter 60 nm) pushed along the supported lipid membrane by an applied buffer flow (10 µL min^{-1}), and the corresponding decomposition into *x*- and *y*-components of the movement (**b**, **c**). Due to the flow, the *x*-component is dominated by directed movement (as indicated by the linear increase over time), while perpendicular to the flow the particle shows only a random movement Note that the different components have different scaling in these plots.

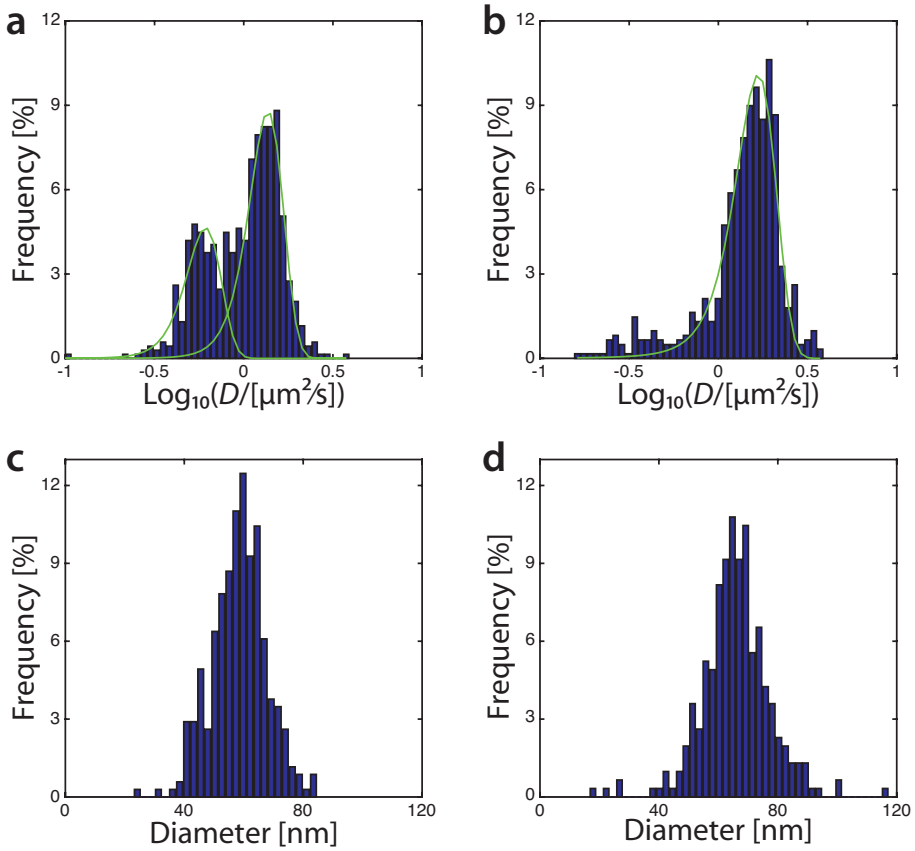

Supporting Figure S7: Diffusivity and size histograms of tracked NPs. Data in (**a**, **c**) were extracted from BACE-positive and in (**b**, **d**) from BACE-negative samples, respectively.

Supporting Method 1

Expression of full-length BACE1 and generation of native membrane vesicles (NMVs). Baculovirus stock containing full-length BACE1 (also including a His-tag) was amplified in Sf21 cells grown in Sf900 II media supplemented with 10% fetal bovine serum (Life Technologies) at 27 °C and 150 rpm. Briefly, cells (500 mL, 1.5×10^6 cells mL^{-1}) were infected at a cell-to-virus ratio of 50:1. The cells were harvested (3400×g for 15 min at 4 °C) one week post infection and the supernatant was collected with a virus titer of 2×10^8 CFU mL^{-1}. The virus stock was stored at -80 °C.

For protein expression, Sf9 or Sf21 cells were infected at mid–log phase (2×10^6 cells ml^{-1}) using a cell-to-virus ratio of 1:2, and harvested 48 h post infection. The cell pellet was washed twice in PBS buffer and stored at -80 °C. For generation of membrane material, the cell pellet was thawed on ice, dissolved in lysis buffer (2×PBS, 1 mM EDTA and protease inhibitor cocktail, Roche) and disrupted using an UltraTurrax T25 (IKA) at 13,000 rpm for 2×20 seconds. Intact cells were removed by centrifugation (1,000×g for 10 min, Beckman Coulter). The membrane material in the supernatant was collected by ultracentrifugation (>100,000×g for 30 min, Beckman Coulter) whereupon the pellet was resuspended in 2×PBS with protease inhibitor cocktail and homogenized with a dounce homogenizer to create native membrane vesicles (NMVs). These were again collected by ultracentrifugation, and the pellet was dissolved in 2×PBS with 20% glycerol. Aliquots of NMVs were snap frozen in liquid N_2 and stored at -80 °C.

Purification of full-length BACE1 NMVs was thawed on ice, solubilized under stirring in 2×PBS with 2% Triton-X and protease inhibitors for 30 min at 4° C and then homogenized with a dounce homogenizer. The soluble fraction was separated from the insoluble fraction by ultracentrifugation (>100,000×g for 30 min). Full-length BACE1 was purified on two affinity columns with immobilized Ni^{2+}-NTA and a substrate analogue inhibitor,[1] respectively. Briefly, a 5 mL HiTrap HP column (GE healthcare) was equilibrated in buffer A (2×PBS, 0.1% Triton-X) supplemented with 3% of buffer B (2×PBS, 0.1%

Triton-X, 0.4 M imidazole, pH 7.4) on a ÄKTA purifier (GE healthcare). After sample application (1.5 mL min^{-1}), the column was washed first with buffer supplemented with 3% of buffer B, followed by buffer supplemented with 8% of buffer B, and finally by 100% of buffer B to elute the protein. The eluate was pooled and the buffer was exchanged for 25 mM NaAc, 100 mM NaCl, 0.1% Triton-X, pH 4.5, using PD-10 columns (GE healthcare). A visible precipitate formed during the process was removed by centrifugation (4,000×g for 15 min at 4 °C). The sample was applied to an equilibrated column containing BACE1 substrate analogue inhibitor (Thermo Fischer), covalently coupled to NHS-activated sepharose beads (GE healthcare). After sample application (2 mL min^{-1}), the column was washed before eluting in 2×PBS, 0.1% Triton-X, pH 7.4. Due to interference between protein and Triton-X with respect to light adsorption at λ=280 nm, protein concentration was estimated from the intensity of the BACE1 band on a gel by comparison with a BSA ladder of known concentrations. Aliquots of NMVs were snap frozen in liquid N_2 and stored at -80°C.

SDS-PAGE and Western blotting. NMVs and purified protein was supplemented with 4×LDS buffer and loaded on 12-well NuPAGE 4-12% Bis-Tris SDS-PAGE gels (ThermoFischer). A SHARP pre-stained marker (ThermoFischer) was included in row 1 and 12. The gels were run in 1×MES buffer for 40 min at 200 V. For Coomassie staining, one gel was transferred to Instant Blue (Expedeon) until visible bands appeared. For Western blot, the proteins were transferred to the PVDF membrane using Trans Blot Turbo (Bio-RAD) and blocked in PBS supplemented with 1% BSA for 5 min before addition of primary (anti-His_6) and secondary (anti-mouse-AP conjugate) antibodies (Promega), which were incubated overnight. The blot was washed 3 times in PBS with 0.1% Tween20, and 3 times in PBS, followed by development using One-step developer (ThermoFischer) until the bands were clearly visible.

Western blot (see Supporting Fig. 1) clearly indicated expression of BACE1 in NMVs obtained from transfected cells, in contrast to mock membrane obtained from similar but not transfected cells where BACE1 was absent. The

BACE1 content in the NMVs was estimated from the blot intensities (indicated by arrows in Supplementary Figure 1) to >0.125 µg BACE1 per 300 µg NMVs.

Biotinylation of purified BACE1 and reconstitution into synthetic vesicles. Purified, detergent-solubilized BACE1 was biotinlyated by addition of 10 times molar excess of Sulfo-NHS-LC-Biotin (EZ-Link, Thermo Scientific), followed by over-night incubation at 0 °C. To enable measurement of the degree of biotinylation from the absorption at λ=260 nm without interfering adsorption from Triton-X, a buffer exchange was performed before the biotinylation where 2×PBS with 0.1% Triton-X was exchanged for 2×PBS with 0.1% Triton-X Red. The average number of biotins added to each BACE1 was determined from the difference in absorption at λ=260 nm before and after incubation (corrected for spontaneous hydrolysis in the PBS sample), assuming a molar absorptivity of ε=9,700 $M^{-1}cm^{-1}$ for the NHS-leaving group released during conjugation. Using this procedure, the degree of biotinylation was estimated to approximately 1 biotin per BACE1. Excess Sulfo-NHS-LC-biotin and by-products released during conjugation were removed by five sequential separations over a 5 kDa cut-off spin column (Illustra MicroSpin).

Biotinylated BACE1 was reconstituted into liposomes made from 1-palmitoyl-2-oleoyl-*sn*-glycero-3-phosphocholine. Lipids were dissolved in chloroform in a round-bottom glass flask, whereupon the solvent was evaporated to form a thin lipid film. This lipid film was rehydrated in sodium acetate buffer (100 mM NaAc, 200 mM NaCl, pH 4.5, 10 mM Triton-X100), and the so-obtained mixed micelles were stored at 4°C. Detergent-solubilized BACE1 (0.05 mg mL^{-1}) was mixed with the micelles in a protein-to-lipid ratio of 1:1000. To slowly remove the detergent, MilliQ water-washed Biobeads SM2 (Bio-Rad) was added to the micelle solution, which was incubated overnight under gentle mixing. The reconstitution process was monitored by dynamic light scattering (APS zetasizer, Malvern); the initial protein-containing micelles showed a narrow size distribution with average size 8±2 nm. Detergent removal with Biobeads led to the formation of liposomes with average size 130±50 nm. The reconstitution efficiency was estimated to be 30–70% using an enzymatic assay.

Supporting Method 2

Gold nanoparticle (NP) synthesis. NPs approximately 50 nm in diameter were synthesized by seed-mediated synthesis.[2,3] NP seeds were prepared by citrate reduction of chloroauric acid, which proceeded by heating 200 mL aqueous solution of $HAuCl_4$ (0.5 mM) to boiling whereupon 10 mL aqueous solution of sodium citrate (38.8 mM) was added. The mixture was then continuously boiled until after approximately 20 minutes a ruby-red colour had developed. Seed-mediated growth was then performed at room temperature with ascorbic acid as reducing agent. An aqueous solution of 4 mL $HAuCl_4$ (20 mM), another aqueous solution of 0.4 mL $AgNO_3$ (10 mM) and finally 15 mL of the pre-prepared seed NPs were all added to 170 mL MilliQ water. An aqueous solution of 30 mL ascorbic acid (5.3 mM) was then added to the solution containing the seed NPs at a rate of 600 µL min^{-1}, controlled by a syringe pump (NE-1000, New Era Pump), under constant stirring.

The size distribution of the synthesized NPs was determined from micrographs obtained with a Zeiss Ultra 55 FEG Scanning electron microscope (see Supporting Figure 2). Samples for SEM analysis were prepared by adsorption of citrate-stabilized NPs to silicon surfaces modified with 3-aminopropyldimethyl ethoxysilane, making the silicon substrates positively charged. Prior to adsorption, NPs were concentrated by centrifugation and transferred to a dilute citric buffer (ionic strength <1 mM) in order to increase the electrostatic repulsion between neighbouring NPs, thereby minimizing aggregation of NPs during drying of sample surfaces. Distributions of projected areas of supported NPs were extracted from micrographs obtained at different magnifications using the public domain image processing software ImageJ and the built-in “analyse particles” tool. The concentration of NP in the original particle sol was determined to 0.1 nM, calculated based on the average NP volume, the total amount of gold atoms in the synthesis, and tabulated values for gold molar volume.

Gold NP surface functionalization. The citrate-stabilized NPs were surface functionalized in aqueous solution from a mixture of thiolated poly(ethylene)

glycols (PEG) containing α-hydroxy-ω-mercapto-PEG, α-carboxy-ω-mercapto-PEG and α-biotinyl-ω-mercapto-PEG (MW 5 kDa; RAPP Polymere, Germany). As detailed somewhere else,[4] the ratio of the different thiolated PEG were adjusted to give on average a single biotin ligand per NP, which for a gold NP with diameter of 50 nm is achieved for a relative content of 0.0125 % α-biotinyl-ω-mercapto-PEG. The mixture of AuNPs and ω-mercapto-PEG was incubated over night, after which surplus thiolated PEG was removed through filtration using centrifuge filter columns with 300 kDa-cut off (PALL, USA).

Assembly of antibody-NP (Ab-NP) constructs. Biotin-functionalized NPs were conjugated to monoclonal antibodies directed towards BACE1 in a two-step procedure *via* Streptavidin (SA) coupling. SA was first conjugated to the biotin-functionalized NPs by slow addition of NPs to a stirred solution of SA in PBS (pH 7.4) supplemented with 0.1 mg mL^{-1} BSA. The concentration of SA was adjusted to reach a final excess of ~1,000 SA per added NP. Typically, to make 500 µL solution of NP-SA complexes with particle concentration 1 nM, 250 µL NP solution (2 nM) were added to 250 µL SA solution (2 µM) at a rate of 5 µL min^{-1}. After conjugation, excess SA was removed by five sequential filtration steps using centrifuge-filter columns with 300 kDa cut-off. As determined from dynamic light scattering-measurements obtained with a Malvern Zeta Sizer NanoZS instrument, SA conjugation according to this protocol did not induce aggregation of the biotin-functionalized NPs. SA-conjugated NPs (SA-NP) were used for initial characterization experiments with Evanescent Wave Scattering Microscopy (EvSM, *cf.* Supporting Method 4) and for separation experiments where reconstituted and biotinylated BACE1 was employed. SA-NPs were also used for conjugation of antibodies directed towards the ectodomain of BACE1.

Antibodies [Ab, BACE1 monoclonal antibody (M01), clone 2C1, Abnova] were biotinylated by addition of 10 times molar excess of Sulfo-NHS-LC-Biotin (EZ-Link, Thermo Scientific) in PBS buffer, incubated at room temperature for 1h. The average number of biotins added to each antibody was determined from the difference in absorption at λ=260 nm before and after incubation

(corrected for spontaneous hydrolysis in the PBS sample), assuming a molar absorptivity of ε=9,700 $M^{-1}cm^{-1}$ for the NHS-leaving group released during conjugation. This procedure showed that conjugation with 10 times excess Sulfo-NHS-LC-Biotin resulted in 2 biotins per Ab. Excess Sulfo-NHS-LC-Biotin and by-products released during conjugation were removed by two sequential runs through a micro-spin column (Illustra MicroSpin).

The biotinylated Ab were conjugated to SA-NPs by slow addition of SA-NPs to a solution containing biotinylated Ab in PBS supplemented with BSA (0.1 mg mL^{-1}). The Ab concentration was adjusted in order to maintain excess corresponding to 100 Ab per added SA-NP. Typically, to get 500 µL Ab-NP solution (1 nM), 250 µL SA-NP solution (2 nM) was added at a rate of 5 uL min^{-1} to 250 uL solution of biotinylated Abs (200 nM). After conjugation, surplus of antibodies were removed by three sequential washing steps using centrifuge filter columns. High concentration of free protein in the vesicle solution can potentially lead to problems with the formation of supported membranes. Therefore, PBS without added BSA was used to dilute the Ab-NPs after the final washing step.

Supporting Method 3

Assembly of Ab-NP-NMV constructs. To introduce PEGylted lipids into NMVs, these were mixed at ratio 1:10 with synthetic dilution vesicles (SUVs) and the mixture was sonicated for ten minutes at 20°C in an ultrasonicator (S40H, Elmasonic).[5] The PEG-containing SUVs were made from 99 mol% 1-palmitoyl-2-oleoyl-sn-glycero-3-phosphocholine (Avanti Polar Lipids) and 1 mol% 1,2-dipalmitoyl-sn-glycero-3-phosphoethanolamine-N-[methoxy(polyethylene glycol)-2000] (ammonium salt) (Avanti Polar Lipids) by extrusion through a 50 nm filter (Whatman).[6,7]

The sonication-treated NMVs were mixed with the Ab-NP constructs at an estimated ratio of 1 Ab-NP per BACE1 and incubated over night at 8°C. The resulting Ab-NP-NMV constructs were visualised by TEM. Electron

micrographs were recorded on a FEI Tecnai G2 microscope operated at 160 kV acceleration voltage using formvar- and carbon-coated cupper grids (FCF300-Cu-TB, Electron Microscopy Sciences, USA). These were first hydrophilized by UV/Ozone treatment for 5 minutes (ProCleaner, Bioforce Nanoscience) and then either used as is, or further treated with poly-L-lysine (PLL) applied by positioning the grid on a droplet of PLL solution (20 µg mL^{-1} in MilliQ water). Treated grids were positioned on top of droplets containing Ab-NP-NMV solution for 15 minutes, whereupon adsorbed material was fixed by reaction with glutaraldehyde (2.5% in PBS) for another 15 minutes. After fixation, grids were carefully rinsed and blotted three times, whereupon the samples were stained with uranylacetate (1% in MilliQ water) for 60 seconds. Supplementary Figure 3 display a small selection of electron micrographs showing the same sample adsorbed onto grids without and with PLL-modification, respectively. Grids without PLL coating were only sparsely covered by seemingly intact NMVs whereas the positively charged PLL-modified grids were covered with collapsed or partly collapsed vesicles. Nanoparticles could be seen attached to some of the adsorbed vesicles, and in most cases only one particle was associated to a single vesicle.

Supporting Method 4

Evanescent wave scattering microscopy (EvSM). The adsorption of Ab-NP-NMVs to a glass surface and their transformation to a supported lipid membrane was monitored by EvSM. The principle of this method and the fabrication of the waveguide chip employed are described in detail somewhere else.[8] Briefly, measurements were done with a hybrid waveguide chip consisting of a 500-nm core of SiO_2 (spin-on-glass, IC1-200, Futurrex Inc.) cladded on each side by a 4 µm-thick layer of polymer (CTX-809AP2, AGC Chemicals, ASAHI Glass Co., LTD.) A single-mode, polarization-maintaining optical fibre (P460-HP from Thorlabs) was used to couple 532 nm TE polarized laser light (NANO 250, QiOptiq) into the waveguide using a micrometre stage. A well formed in the upper cladding layer, thereby exposing the glass core layer, enabled illumination of sample close to the bottom of the

well by the evanescent light at the glass-liquid interface. The waveguide chip and the alignment mechanism was placed on an upright Olympus X61 microscope, equipped with a 100× magnification, NA=1.0 water immersion objective (Zeiss), and a Hamamatsu ORCA-Flash4.0 V2 digital CMOS camera for image acquisition. The translational stage, microscope, and camera were controlled using the open-source software MicroManager. Ab-NP-NMVs were injected into a droplet of buffer applied in the sample well whereupon their adsorption to the glass interface and rupture were recorded (see Supporting Movie 3).

Supporting Method 5

BACE1-accumulation: set up and procedures. A 4-arm microfluidic device (Supplementary Figure 5) was made of polydimethylsiloxane (PDMS) from a mixture of 10:1 Sylgard 184 and curing agent (Dow Corning) using replica molding.[9,10] Access holes were punched through the PDMS in the connection chambers. The PDMS mold was bonded to a Nanolane T-Surf (pre-cleaned in a 2% Liquinox solution at 80°C for 30 min) after treatment of both the PDMS mold and the Nanolane surface with oxygen plasma. Silicone tubings (1.5 mm ID, VWR Sweden) were glued to the access holes using silicone adhesive (Elastosil A07 RTV-1 silicone rubber, Wacker Silicones, Munich, Germany).

The microfluidic device was mounted on an inverted fluorescence microscope (Eclipse Ti-E, Nikon, Japan) and monochromatic polarized light λ=525 nm (CoolLED) was incident on the Nanolane T-Surf at an angle of approximately 30° through a 60× magnification, NA=1.49, TIRF objective (Nikon). The reflected light was directed to a CMOS camera (Andor Neo, Andor, Ireland) via an analyzer (Nikon) and a 1.5× magnification lens. To enable automated single-particle analysis, in these accumulation experiments Ab-NP-NMVs were diluted 1:20 with SUVs (*cf.* Supporting Method 3). The mixture [diluted in TRIS buffer 10 mM (pH 8.0) and 100 mM NaCl to approximately 0.1 mg mL^{-1} of membrane material] was injected into the microfluidic device. For membrane formation, the mixture was injected into connection 1, a counter

flow was applied to connector number 4, and connection 2 and 3 were used as outlets (see Supporting Fig. 5). This way a supported membrane was formed that covered only the floor on the inlet side of the device with a well-defined bilayer edge at the centre of the device.

After completed membrane formation, excess vesicles were removed by extensive rinsing with Tris buffer, whereupon the flow configuration was changed by closing connections 2 and 3 and open connection 4. The resulting flow, this way directed along the lipid membrane towards the membrane edge, pushing the mobile NPs accordingly, gave rise to accumulation of NPs at the membrane front.

Control experiments were performed similarly, but BACE1-containing NMVs were replaced either by negative control NMVs (from cells not expressing BACE1) or by vesicles with reconstituted BACE1. In all cases, the process was recorded by acquiring movies at 20 fps using an exposure time of 30 ms and the “Acquire Fast Timelapse” function in NIS Elements (Nikon) (see Supporting Movie 4).

Supporting Method 6

Single particle tracking analysis. Data analysis was done with MatLab (MathWorks, Natick, USA) employing dedicated scripts for single particle tracking based on local nearest-neighbour linking.[11] For nanoparticles under flow, we observed trajectories showing a superposition of random walk and directed movements. In theory, the directed movement is fully restricted in direction of the flow (denoted as *x*-axis in the following), while the movement perpendicular to the flow (*y*-axis) is expected to be purely random. This is well illustrated in Supporting Fig. 6, displaying a representative trajectory and its decomposition into *x*- or *y*-coordinates: while the *y*-component shows only random fluctuations, a superposition of linear increase and random fluctuations is observed in the *x*-component.

To extract the 2D diffusion coefficient, *D*, and the size of each tracked particle, the method presented by Block *et al.*[12] was employed where *D* was calculated using the internal averaging procedure[13] corrected for motion blur.[14] Briefly, the recorded tracks were decomposed into *x*- and *y*-components where the *x*-component was further deconvoluted into deterministic and stochastic components. Both the deterministic and the stochastic movements of the NPs contain information about their linker properties (*i.e.* in this case the strength of the frictional coupling between the BACE1 protein and the lipids). By extracting this from the stochastic movement, the force acting upon the NP can be extracted from the deterministic.[12] With the force being proportional to the surface area of the NP, the NP size can be calculated. By analysing tracks longer than 75 frames, an estimated relative accuracy of 13% in the determination of *D* was achieved.[15] Examples of size and diffusion histograms obtained from experiments with BACE1-conataining NMVs and mock NMVs are displayed in Supporting Fig. 8, respectively. While the BACE1-positive sample displays two distinct peaks in the diffusivity histogram, only one peak is visible in the size distribution. In contrast, the BACE1-negative sample shows only one peak in both histograms.

Supporting Discussion 1

Design criteria for nanoparticles. In order to work properly for membrane-protein purification, NPs must be engineered to fulfill the following criteria:

i) The active translation of membrane protein requires the use of NPs orders of magnitude larger than the protein themselves, i.e. hydrodynamic diameter ~30-50 nm or larger.
ii) The NPs must not have a significant affinity to the lipid membrane in that they to large extent bind non-specifically and compromise the membrane integrity.
iii) The NPs must bind to the targeted membrane proteins in such way that the protein and membrane mobility is not obscured.
iv) Since, for practical reasons, NP concentration and interaction time are limited, a reasonable high targeting efficiency must be achieved.

In this work, we chose to use NPs with hydrodynamic diameter of ~60 nm. This means that the flow-exposed area of each NP is approximately two orders of magnitude larger than the corresponding area of the membrane proteins. Accordingly, the applied flow could be decreased about two orders of magnitude. Though, a specific drawback of using larger NPs is that non-specific interactions between NP and lipid membrane increase with NP size. This is true for long-distance interactions, mainly van der Waals and electrostatic forces, but also for shorter-ranged forces due to direct contact between a lipid bilayer and a NP; Larger particles have a larger contact area, and the lipid bilayer can more easily accommodate, i.e. bend, around objects with lower curvature. It is well known that the uptake of NPs by cells increase significantly when nanoparticle size increase from ~10 nm to ~60 nm.[16]

By modifying the surface of the gold NPs with a monolayer brush of PEG (MW 5 kDa), where every third PEG-molecule displayed peripheral carboxylic acids, these particles yielded colloidal stability and neglectable non-specific binding to model lipid membranes made up by zwitterionic POPC lipids under

a wide range of buffer conditions.[4] This is due to a combination of repulsive steric and hydration forces between the lipid bilayer and the PEG-brush, as well as electrostatic double layer interaction between the negatively charged nanoparticles and slightly negatively charged lipid membrane.

We also prepared similar NPs with addition of a varying number of peripheral biotin, from single to several hundred per NP.[4] The influence of the number of biotin ligands per NP on its 2D-diffusivity in a lipid membrane was tested by monitoring with EvSM (see Supporting Method 4) binding of NPs to a lipid membrane modified to display streptavidin. Supporting Movies 1 and 2 show in real-time the addition of NPs carrying 1 and 38 biotinylated PEG ligands (out of totally ~8000 PEG ligands per nanoparticle), respectively. These experiments revealed that only NPs with a single biotin ligand, i.e. monovalent particles, remained mobile over longer time scales, whereas multivalently interacting NPs eventually became completely stuck. This result was surprising in light of previous results obtained for lipid vesicles displaying surface-mobile ligands, where multivalent interaction was found to only to reduce the apparent diffusivity in relation to number of bonds between the vesicle and the lipid membrane.[15] In contrast, for the NPs employed here, having non-mobile, high-affinity ligands, we could confirm, from these and other complementing experiments, that the lipid bilayer bends around the NP, causing its immobilization. Based on this insight, we here used antibody-modified NPs containing monovalent biotin-functionalized gold-PEG NPs as template, since this allowed facile control of the number of antibodies conjugated to each particle.

While monovalent NPs provide unconstrained mobility, they may suffer from low targeting efficiency. This can be understood considering that for NPs carrying affinity ligands that form strong bonds, e.g. antibodies, targeting performance is likely limited by the rate of bond formation. To a first approximation, this rate decreases in proportion to the NP concentration, the concentration of target (in the present case BACE1) and the coverage of affinity ligands (in the present case antibody) on the surface of the NP. For NPs where the non-reactive surface is large compared to the area covered by

the affinity ligand, as is the case for a nanoparticle 60 nm in diameter carrying a single antibody, the latter is low, ~1% or less depending on the mode of antibody conjugation. Thus, these NPs may form bonds at rates orders of magnitude slower than would unconjugated antibody applied at the same concentration. (A theoretical model and experimental support for these reasoning can be found in reference 4). Furthermore, for larger NPs like those employed here, the applicable NP concentration is for practical reasons (high sample consumption and too strongly scattering solutions) usually less than 100 pM, which is at least two orders of magnitude below the antibody concentration commonly employed in immunohistochemistry.

In an attempt to improve the targeting efficiency, we let antibody-modified NPs react with BACE1 as these remained in vesicles, in a test tube prior to membrane formation. This approach turned out to be advantages, presumably since reaction occurred at several orders of magnitude higher concentrations of membrane protein and NPs, respectively, as neither of the reactants were diluted before mixing. Furthermore, this procedure also conveniently allows targeting to take place for longer time, e.g. over night.

Supporting Discussion 2

Origin of immobile nanoparticles. In the process of transferring membrane protein (BACE1) from the cellular membrane to a supported membrane, at least two steps can be recognized where proteins are potentially “lost”. In a first instance this may occur when the cellular membrane is turned into NMVs, and the ectodomains of the proteins end up at the inside of these. Since in our assay NP targeting directed towards the protein ectodomain is taking place outside the vesicles, those membrane proteins are non-targetable.

In a second instance proteins may end up with their ecdodomain facing the solid support under the lipid membrane as the NMVs rupture. This has indeed been experimentally verified for BACE1 coming from the same source as used in this work: Pace *et al.*[5] used two different fluorescent probes with affinity for the ectodomain and the cytosolic domain of BACE1, respectively,

and showed that after NMVs rupture, BACE1 existed in the lipid membrane both with the ectodomain at the glass-membrane and at the water-membrane interface, although quantitative estimates of the different directions were not made. From measurements of fluorescence recovery after photo bleaching (FRAP), it was further shown that ~25% of BACE1 directed with their ectodomain away from the distal membrane leaflet remained immobile after membrane formation, which was attributed mainly to the presence of unrupted NMVs. Under the assumption that the presence of NPs does not influence the tendency of vesicles to rupture, one would thus assume a similar fraction (~25%) of immobile NPs as measured for fluorescently labelled BACE1 with FRAP. Yet, in our experiments the fraction of immobile NPs is at least twice as high.

To understand the origin of the apparent surplus of immobile NPs, we scrutinized the membrane-formation stepwise in a protein-free setting using EvSM. This was done by sequentially injecting onto a clean glass surface first low concentration of gold-PEG NPs and then lipid vesicles purely made from POPC lipids. These measurements showed that under the high ionic strength conditions applied in our experiments, i.e. in the absence of electrostatic double-layer repulsion, the gold-PEG NPs bound irreversibly to the glass support (Supporting Movie 5, the same experiment with higher applied NP concentration is shown in Supporting Movie 6).

Supporting Movie 7 show the same surface upon addition of lipid vesicles. Due to their much lower scattering compared to the gold-PEG NPs, scattering from single vesicles is barely visible, but binding can be identified from t~50 seconds as a continuous increase of the background intensity. At t~1:30 background intensity start decreasing as vesicles rupture and at t~2:00 a lipid membrane has formed on the floor around the immobilised NPs. With few exceptions, the NPs remained immobile during and after membrane formation; occasionally a particle left the surface after membrane formation and, interestingly, few particles also displayed a limited 2D-mobility in the surface plane, which can be seen at the very end of the movie. After formation of a lipid membrane, no further binding of gold-PEG NPss was observed, also

when higher NP concentration was applied as shown in Supporting Movie 8, acquired at high frame rate.

From this experiment, we conclude that the magnitude of immobile NPs observed after formation of a lipid membrane from a mixture of NMVs and NPs may relate to NPs that bind to the underlying glass substrate. These contacts may be created during rupture of the NP-NMV complexes, but also prior to NMV rupture due to complexes adsorbing with the NPs facing the glass substrate. From geometrical considerations, assuming NMVs with radius 75 nm and gold-PEG nanoparticles with radius 30 nm, the latter is expected to occur with at least 20% probability. In addition, the mixture of NMVs and targeted NPs likely contain a fraction of “free” non-bound NPs that may adsorb to the glass surface independently of the NMVs. Furthermore, the experiment, performed in a protein-free setting, confirms that the non-specifically bound, 2D-mobile nanoparticles present in all experiments and characterized by the same high diffusivity of single lipids, indeed appear due to contact between the nanoparticle itself and some lipid-sized component of the membrane, although the tiny details of this interaction remain unclear.

Supporting Movies

Supporting Movie 1: EvSM of binding of monovalent gold-PEG-biotin NPs to streptavidin-modified lipid membrane. The movie shows the binding of monovalent gold-PEG-biotin NPs (average core diameter 50 nm and on average 1 biotin per NP) to a supported lipid membrane modified to display streptavidin. The streptavidin was bound to biotinylated lipids [1,2-Dioleoyl-sn-Glycero-3-Phosphoethanolamine-N-(biotinyl), 0.025%] diluted in a background of zwitterionic POPC lipids. NPs are applied at a concentration of approximately 20 pM. After binding, most NPs display 2D mobility. The movie is acquired at 15 frames per second. The full frame size is 50x50 μm^2.

Supporting Movie 2: EvSM of binding of multivalent gold-PEG-biotin NPs to streptavidin-modified lipid membrane. The movie shows the binding of multivalent gold-PEG-biotin NPs (average core diameter 50 nm and on average 38 biotins per NP) to a supported lipid membrane modified to display streptavidin. The streptavidin was bound to biotinylated lipids [1,2-Dioleoyl-sn-Glycero-3-Phosphoethanolamine-N-(biotinyl), 0.025%] diluted in a background of zwitterionic POPC lipids. NPs are applied at a concentration of approximately 20 pM. After binding, NPs do not show 2D-mobility. The movie is acquired at 15 frames per second. The full frame size is 50x50 μm^2.

Supporting Movie 3: EvSM of lipid membrane formation by adsorption and rupture of Ab-NP-NMV constructs. The movie shows the rupture of Ab-NP-NMV constructs (see Supporting Method 3 & 4 for the experimental details) on a clean glass surface. After membrane formation, about 50% of the immobile NPs show 2D mobility. The film is acquired at 1 frame per second. The full frame is 100x100 μm^2.

Supporting Movie 4: SEEC microscopy of flow-induced NP transfer in a lipid membrane. The movie shows the flow-induced transfer of NPs bound to a lipid membrane made by rupture of Ab-NP-NMVs (see Supporting Method 3 & 5 for the experimental details) on the floor of a microfluidic channel. The movie is acquired at 30 frames per second. Scale bar is 10 μm.

Supporting Movie 5: EvSM of nonspecific adsorption of gold-PEG NPs to glass at low concentration. The movie shows adsorption of gold-PEG NPs (average core diameter 50 nm) to a clean glass surface. The movie is acquired at 0.5 frame per seconds and the concentration of NPs in solution is gradually increased from 0 to approximately 500 fM during the length of the movie. Scale bar is 20 μm.

Supporting Movie 6: EvSM of nonspecific adsorption of gold-PEG NPs to glass at high concentration. The movie shows adsorption of gold-PEG NPs (average core diameter 50 nm) to a clean glass surface. The movie is acquired at 0.5 frame per seconds and the concentration of NPs in solution is gradually increased from 0 to approximately 20 pM during the length of the movie. Scale bar is 20 μm.

Supporting Movie 7: EvSM of the formation of supported lipid bilayer around surface-bound gold-PEG NPs. The movie shows gold-PEG NPs (average core diameter 50 nm) nonspecifically adsorbed to a glass surface at t = 0 sec. At t= 48 sec a 0.2 ug/ml POPC vesicle solution (average vesicle diameter 50 nm) is introduced and at t= 51 sec, individual vesicles start arriving to the surface. The concentration of surface-adsorbed vesicles gradually increases until a critical surface coverage is reached at around t = 1m 40 sec, at which point the vesicles rupture and fuse to form a supported lipid bilayer. After the formation of supported lipid bilayer is complete, few of the surface-adsorbed NPs become mobile, but most remain immobile on the surface. The movie is acquired at 1 frame per second. Scale bar is 20 μm.

Supporting Movie 8: EvSM of gold-PEG NPs bouncing on supported lipid bilayer. The movie shows gold-PEG NPs (average core diameter 50 nm) at 20 pM, diffusing in and out of the evanescent field close to the supported lipid bilayer surface. The NPs do not adsorb but bounce off the supported lipid bilayer. The immobile NPs seen on the surface were adsorbed prior to formation of supported lipid bilayer. The movie is acquired at 30 frames per second. Scale bar is 20 μm.

References:

(1) Sinha, S.; Anderson, J.; Barbour, R.; Basi, G.; Caccavello, R.; Davis, D.; Doan, M.; Dovey, H.; Frigon, N.; Hong, J.; Jacobson-Croak, K.; Jewett, N.; Keim, P.; Knops, J.; Lieberburg, I.; Power, M.; Tan, H.; Tatsuno, G.; Tung, J.; Schenk, D.; Seubert, P.; Suomensaari, S.; Wang, S.; Walker, D.; Zhao, J.; McConlogue, L.; John, V. *Nature* **1999,** 402, 537-540.

(2) Park, S.; Yang, P.; Corredor, P.; Weaver, M. *J. Am. Chem. Soc.* **2002,** 124, 2428-2429.

(3) Park, Y.; Park, S. *Chem. Mater.* **2008,** 20, 2388-2393.

(4) Lundgren, A.; Agnarsson, B.; Zirbs, R.; Zhdanov, V. P.; Reimhult, E.; Höök, F. *ACS Nano* **2016,** 10, 9974-9982.

(5) Pace, H.; Nyström, L.; Gunnarsson, A.; Eck, E.; Monson, C.; Geschwindner, S.; Snijder, A.; Höök, F. *Anal. Chem.* **2015,** 87, 9194-9203.

(6) Hope, M. J.; Bally, M. B.; Webb, G.; Cullis, P. R. *Biochim. Biophys. Acta* **1985,** 812, 55-65.

(7) Mayer, L. D.; Bally, M. B.; Cullis, P. R. *Biochim. Biophys. Acta* **1986,** 857, 123-126.

(8) Agnarsson, B.; Lundgren, A.; Gunnarsson, A.; Rabe, M.; Kunze, A.; Mapar, M.; Simonsson, L.; Bally, M.; Zhdanov, V.; Höök, F. *ACS Nano* **2015,** 9, 11849-11862.

(9) McDonald, J.; Duffy, D.; Anderson, J.; Chiu, D.; Wu, H.; Schueller, O.; Whitesides, G. *Electrophoresis* **2000,** 21, 27-40.

(10) Xia, Y.; Whitesides, G. *Annu. Rev. Mater. Res.* **1998,** 28, 153-184.

(11) Meijering, E.; Dzyubachyk, O.; Smal, I.; Conn, P. *Imaging and Spectroscopic Analysis of Living Cells: Optical and Spectroscopic Techniques* **2012,** 504, 183-200.

(12) Block, S.; Fast, B. J.; Lundgren, A.; Zhdanov, V. P.; Höök, F. *Nat. Commun.* **2016,** 7, 12956.

(13) Saxton, M. *Biophys. J.* **1997,** 72, 1744-1753.

(14) Berglund, A. *Phys. Rev. E* **2010,** 82.

(15) Block, S.; Zhdanov, V. P.; Höök, F. *Nano Lett.* **2016,** 16, 4382-90.

(16) Chithrani, B. D.; Ghazani, A. A.; Chan, W. C. W. *Nano Lett.* **2006,** 6, 662-668.